This is a repository copy of *Modelling of bismuth segregation in InAsBi/InAs superlattices: Determination of the exchange energies*.

White Rose Research Online URL for this paper:
http://eprints.whiterose.ac.uk/146061/

Version: Accepted Version

Article:
Flores, S., Reyes, D.F., Braza, V. et al. (6 more authors) (2019) Modelling of bismuth segregation in InAsBi/InAs superlattices: Determination of the exchange energies. Applied Surface Science, 485. pp. 29-34. ISSN 0169-4332

https://doi.org/10.1016/j.apsusc.2019.04.188

Article available under the terms of the CC-BY-NC-ND licence (https://creativecommons.org/licenses/by-nc-nd/4.0/).

Reuse
This article is distributed under the terms of the Creative Commons Attribution-NonCommercial-NoDerivs (CC BY-NC-ND) licence. This licence only allows you to download this work and share it with others as long as you credit the authors, but you can't change the article in any way or use it commercially. More information and the full terms of the licence here: https://creativecommons.org/licenses/

Takedown
If you consider content in White Rose Research Online to be in breach of UK law, please notify us by emailing eprints@whiterose.ac.uk including the URL of the record and the reason for the withdrawal request.

eprints@whiterose.ac.uk
https://eprints.whiterose.ac.uk/

Modelling of bismuth segregation in InAsBi/InAs superlattices: determination of the exchange energies.

S. Flores[1], D. F. Reyes[1], V. Braza[1], R. D. Richards[2], F. Bastiman[2], T. Ben[1], N. Ruiz-Marín[1], J. P. R. David[2] and D. González[1]

[1] University Research Institute on Electron Microscopy & Materials, (IMEYMAT), Universidad de Cádiz, 11510 Puerto Real (Cádiz), Spain.

[2] Department of Electronic and Electrical Engineering, University of Sheffield, United Kingdom.

Abstract

InAsBi dilute alloys are potential new candidates for the improvement of infrared optoelectronic devices such as photodetectors or lasers. In this work, InAsBi/InAs superlattices (SLs) with Bi contents ranging between 1-3% were grown by molecular beam epitaxy with different Bi fluxes and growth temperatures to analyze Bi segregation by cross sectional transmission electron microscopy techniques. Bi segregation profiles have been described layer-by-layer using a three-layer fluid exchange mechanism, extracting the values of the As/Bi exchange energies (E_1, 1.26±0.01 eV and E_2, 1.36±0.02 eV). A relationship to calculate the activation energies for exchange from the binding energies in III-V alloys is proposed, which would allow predicting them for other hitherto unknown compounds.

Keywords: InAsBi, segregation, bismuthide, exchange energies

1. Introduction.

Today there is a continuous need to find new semiconductor materials with more advantageous properties that allow the development of devices currently required in our society. In recent years, there has been an increasing interest for synthetizing new semiconducting materials based on the incorporation of bismuth in several fields such as efficient photo-catalysts [1,2] or spintronic-related devices [3,4]. Indeed, in the case of epitaxial grown III-V ternary compounds, GaAsBi alloys [5,6] have already been used to form the active region in mid-IR light-emitting structures such as LEDs and optically pumped lasers [7,8]. However, the incorporation of Bi into InAs has only recently been

investigated. Certainly, it seems that the addition of small amount of Bi into InAs causes a large bandgap reduction, up to 55 meV/%Bi, making it very useful for developing novel sources of light and photodetectors, operating in the mid- and far-infrared (3-30 µm) wavelength range [9]. Moreover, this compound comprises semiconductor and semi-metal components and, because of that, it is expected to possess a temperature-insensitive band gap [10,11]. All these characteristics make InAsBi a promising compound for bandgap engineering, strain compensation and optoelectronic integration [12].

However, there is a major challenge in the incorporation of high Bi contents in III-V conventional alloys: the large difference of atomic radius between Bi and Ga/In leads to an extremely large miscibility gap and a very small equilibrium solid solubility (less than 0,025%) [13]. As a consequence, Bi alloys tend to exhibit alloy clustering [14], phase separation [15], formation of Bi droplets [16,17], atomic ordering [18], as well as strong Bi segregation to the surface during epitaxial growth. As a result, high incorporations of Bi are also limited and this is often addressed by very low growth temperatures that can also compromise material quality.

Indeed, ternary alloys offer relatively little versatility in the bandgap engineering due to the tight constraint between the lattice parameter and bandgap to be grown pseudomorphically on a given substrate. An alternative design to simultaneously select the desired bandgap energy and lattice constant is the growth of superlattice structures [19], where bandgap engineering can be achieved by varying the superlattice period (layer thickness/composition) and coherent interfacial strain. Most recently, Webster et al [12] have theoretically calculated the miniband structure of III-V-Bi semiconductor superlattices identifying the optimal designs. For InAsBi-based superlattices, they demonstrated that the strain-balanced systems (InAsBi/InAs) provide stronger absorption as a function of transition energy than their lattice-matched (InAsBi/GaSb) counterparts do. In addition, for very long wavelengths (>12 µm), the rate at which this superlattice absorption coefficients decrease with photon energy is significantly less than the bulk ones, indicating that superlattice designs may be preferable to bulk material in terms of absorption efficacy for longer wavelength applications. Precise strain and band structure engineering in InAsBi superlattices (SLs) can be only attainable through a deep understanding of the growth process, which faces important challenges such as controlling Bi segregation along layers and the achievement of abrupt interfaces at the atomic scale.

In this work, Bi segregation in InAsBi/InAs structures were studied by analyzing different superlattice (SL) structures grown under different Bi fluxes and temperature conditions. The Bi distributions were analyzed by using advanced analytical (scanning) transmission electron microscopy ((S)TEM) techniques. Calculations performed using a three-layer fluid exchange (F3LE) model are used to fit the Bi content profiles of the whole structures. Finally, the relationship between the exchange energies of different III-V compounds and their binding energies is discussed.

2. **Method.**

2.1. Materials.

The samples were grown by solid source molecular beam epitaxy (MBE) on InAs (001) substrates. The native oxide was removed at ~ 530 °C before the substrate temperature was lowered to 500 °C for buffer growth. Each sample consists of a 100 nm-thick InAs buffer layer followed by ten InAsBi/InAs periods, each comprising 8 nm InAsBi and 8 nm InAs, grown at a growth rate of 0.68 ML/s, as measured by reflected high energy electron diffraction oscillations and verified by HAADF TEM observations. Following the final InAs layer, the sample was removed without further overgrowth or annealing. The samples have been classified into two groups according to the substrate temperature during InAsBi/InAs superlattice growth. Firstly, 3 samples have been grown at a low substrate temperature (320 ºC), using different Bi beam equivalent pressures (BEPs): 0.928, 1.27 and 1.71×10^{-7} mBar for samples **LGT-LF, LGT-MF** and **LGT-HF** respectively. The second group consists in 1 sample, **HGT-HF**, which has been grown at a higher substrate temperature (350 ºC) with a Bi BEP of 1.71×10^{-7} mBar.

2.2. Characterization techniques.

Structural and compositional analysis was carried out by transmission electron microscopy (TEM) techniques and completed by high-resolution X-ray diffraction (XRD) measurements. The XRD modelling was performed using Bede RADS Mercury software. The model was initialized with estimated layer thicknesses and compositions and then allowed to iterate towards a solution, which was then checked to ensure it was physically meaningful. High Angle Annular Dark Field (HAADF) imaging and Energy Dispersive X-Ray (EDX) were simultaneously performed in STEM mode in a double aberration corrected FEI Titan Cubed Themis operated at 200 kV. The EDX mapping was performed with four embedded Bruker SDD detectors using ChemiSTEM technology and

processed using Velox's software. The XRD analysis was carried out using a Bruker D8 Discover with the Cu $K\alpha_1$ line.

3. **Results.**

3.1. Structural analysis.

Firstly, high resolution [004] ω-2θ X-ray Diffraction (XRD) scans were performed on all the samples and Figure 1 shows the resulting curve for the **LGT-MF** sample. The other samples produced similar curves. Superlattice (SL) peaks around the mean peak are indicative of a good periodicity of the structure and permit calculation of the SL spacing. Interference fringes are visible between the SL peaks. The XRD curves were modelled with a zinc-blende lattice constant of 6.61 Å [20] (Zinc Blende-InBi has not been synthesized) and assuming all the layers to be fully strained. The stress in the layers is taken into account by the simulation software that we use.

Two approaches were taken to modelling the XRD data from each device. In the first approach (lower data in Figure 1), all of the QWs in a given device were assumed to be identical; with this approach it is possible to produce a good fit to the SL peaks, although the interference fringes are poorly fit. In the second approach (upper data in Figure 1),

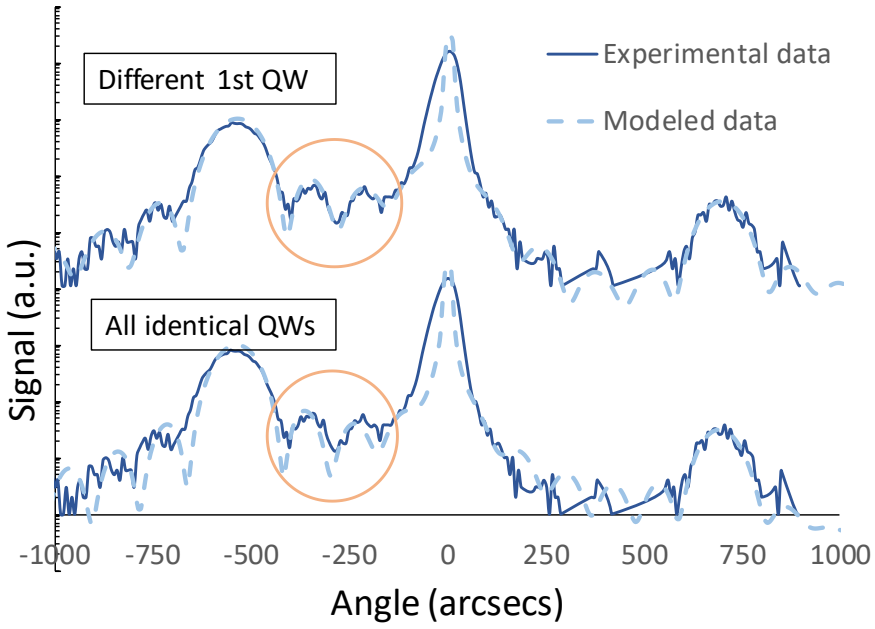

Figure 1. ω-2θ scan of LGT-MF. The experimental scan is presented twice, offset vertically for clarity, with fits from two different models. The lower fit assumes that all 10 QWs in the structure are identical, whereas in the upper fit, the first QW is assumed to be thinner and less Bi rich than the others.

the first QW in a device was assumed to be of lower Bi content and thinner than the

others. With this approach, a better fit to the XRD spectra is obtained (note the better interference fringe fit highlighted in Figure 1), which suggests a better estimation of the overall InAsBi structure thickness.

The results of the average Bi content and the SL spacing from the XRD measurements are shown in Table I. The Bi contents were estimated assuming that all bismuth is concentrated in the InAsBi layers, with a constant composition, and that no Bi is present in the InAs layers. The sample grown at the highest substrate temperature (HGT-HF) evidences the poorest Bi incorporation among the series despite being subjected to the highest Bi flux. Samples grown at the lower temperature show better Bi incorporation, which increases with the Bi cell temperature up to a saturated content of 2.8%. It seems that this marks the solubility limit at this growth temperature.

Table I. Device structure parameters derived from XRD, EDX, and HAADF experiments. The Bi contents and layer thicknesses can be varied by ~0.1% Bi and 0.1 nm in the XRD simulations while still maintaining a reasonable fit to the original spectrum.

	LGT-LF	**LGT-MF**	**LGT-HF**	**HGT-HF**
XRD	All QWs (**model 1**)			
Bi content (%)	2.2	3.4	3.4	1.6
Thickness (nm)	10.3	10.3	9.7	8.5
	Average (**model 1**)			
Bi content (%)	1.5	2.3	2.4	1.0
Period (nm)	15.1	14.9	14.2	13.5
	First QW (**model 2**)			
Bi content (%)	0.3	0.9	2.5	0.6
Thickness (nm)	12.1	11.6	10.1	9.9
	Remaining 9 QWs (**model 2**)			
Bi content (%)	2.2	3.4	3.5	1.6
Thickness (nm)	10.3	10.3	9.7	8.5
	Average (**model 2**)			
Bi content (%)	1.5	2.2	2.3	1.0
Period (nm)	15.1	14.9	14.2	13.5
EDX	Remaining 9 QWs			
Bi content (%)	2.2	3.1	2.9	1.8
HAADF	Average			
Period (nm)	15.6	15.3	14.4	13.7

However, as with other dilute bismuthide alloys, the barriers are not likely to be completely free of Bi. In order to determine the crystalline quality of the samples and the Bi distribution, cross sectional electron transparent samples for TEM were prepared by

conventional techniques for subsequent analysis at the pole [110]. Imaging by conventional TEM under 220BF conditions (not shown here) evidenced all samples were free of extended crystalline defects such as dislocations or planar defects so it could be considered as a pseudomorphic growth. This is in agreement with the boundary conditions used in the simulations of the XRD curves.

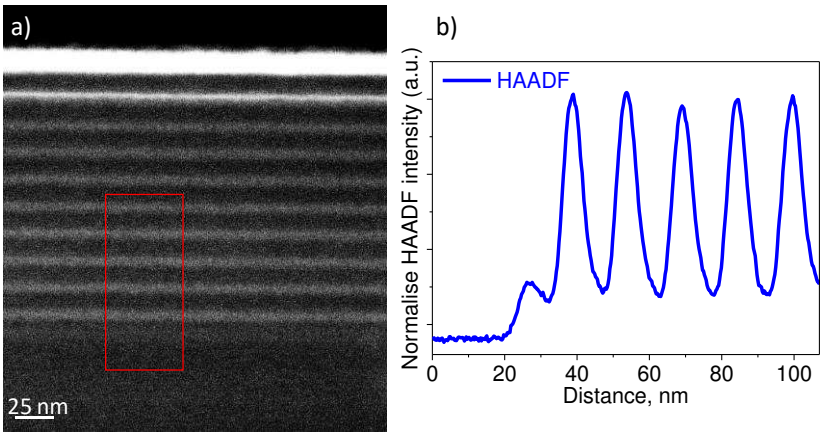

Figure 2. a) HAADF image of sample LGT-MF and b) average HAADF intensity profile along the growth direction. The high contrast in the HAADF image in Figure 2.a) over the 10th layer does not correspond to a high increase in Bi content but comes from a surface contamination of O and Cu in this sample.

Additionally, HAADF imaging was employed to analyse the SL structure since it gives atomic number (Z) contrast images due to the collection of Rutherford-like scattering [21]. In this way, a greater intensity in the image is usually associated with the presence of heavier atoms and, in our case, a higher Bi content, since Z_{Bi}=83 is much higher that Z_{As}=33. Figure 2.a shows a HAADF image of sample LGT-MF, where InAsBi layers can be clearly highlighted due to a higher intensity than the InAs barriers. Notably, the theoretically Bi-free layers between the layers of InAsBi (InAs barriers) in the SL have a much higher intensity than the InAs substrate. That means that the presence of Bi never vanishes throughout the entire SL structure. To evaluate the abruptness of the interface and the correct formation of the designed SL, the average intensity profile along the growth direction is plotted in Figure 2.b, which has been normalized to take into account the thickness gradient of the TEM sample. The profile is far from the nominal square-shape wave, instead following a sinusoidal wave. Singularly, the first layer has a much lower intensity than the second one, but from there on, the intensity profile follows an almost perfect periodicity. This behaviour is repeated for all the samples and was to be expected due to the strong tendency of bismuth to surface segregate, which can cause a variation from the initial design of the nanostructures. The measurements of the SL

periodicity are in good agreement with the XRD results (see the results in Table I). Note that the best fit to the XRD data was provided by a model that assumed a thinner, lower Bi content in the first QW.

In order to provide detailed information about the composition distribution of Bi, EDX maps were acquired from each sample in STEM mode (Figure 3). We use a colour LUT scale to define the Bi content, where the black colour corresponds to null and white the maximum content. First, the comparison of the samples grown at the same growth temperature (320 ºC), but with different fluxes (LGT-LF, LGT-MH and LGT-HF) pointed to an enhancement of the abruptness of the interfaces as the Bi flux increases. The Bi incorporation appears to reach an equilibrium from the second InAsBi layer in each

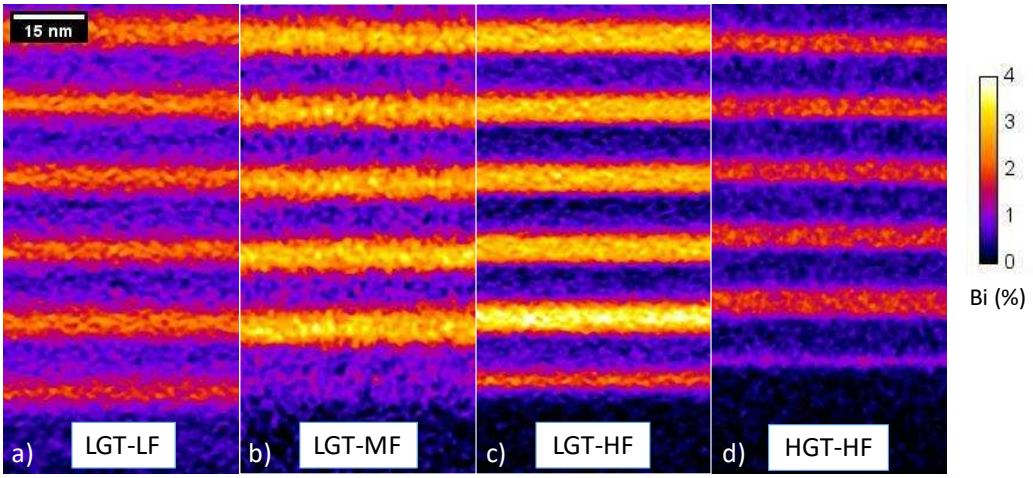

Figure 3. EDX maps of Bi for samples LGT-LF a), LGT-MF b), LGT-HF c) and HGT-HF d).

sample, as can be seen in Figure 3. On the other hand, the comparison of samples grown with the same flux but different growth temperatures (LGT-HF and HGT-HF) revealed a better incorporation of Bi and higher homogeneity when the growth temperature is lower. Therefore, the increase of the growth temperature produces a strong reduction in Bi incorporation. The average Bi contents according to the EDX measurements are slightly higher than the values obtained by XRD (see Table I).

3.2. Modelling the Bi surface segregation.

A suitable model of Bi segregation would help to understand and anticipate the concentration profiles obtained during the growth of InAsBi/InAs heterostructures. In general, the models of segregation in III-V epitaxial growth assume that segregation occurs only between the growing layer and the one immediately below (two-layers

models), as in the exchange model, [22], the kinetic model [23] or the thermodynamic model [24]. Taking into account the nominal values and after making a sweep of different values of the segregation constant in two layer models, we do not get a good adjustment for our results. In fact, it was necessary to modify the constant R and the initial flux to describe the different behaviors that occur between the first and subsequent layers so it was impossible to obtain a good fit of the whole structure. Recently, it has been demonstrated that the fluid three-layer exchange (F3LE) model proposed by Godbey and Ancona [25] could offer the best description of Sb behavior [26,27] and Bi alloys present more similarities in their behaviour with those of Sb than with those of In. In the following, we will apply the F3LE model to simulate the average composition profiles of Bi along the growth direction of the whole SL structure. It also will permit us to obtain thermodynamic parameters unknown for these alloys such as the exchange energies during the surface segregation.

In all the models, segregation is determined by the atomic exchange between the surface layer (s) and the subsurface layers (s-n), assuming only layer-by-layer growth. The evolution of the number of atoms incorporated is given by the balance of incoming and leaving atoms. There is an exchange process from the inner to the surface layer governed by a probability of exchange, P_1, defined by an energy barrier E_1 as $\boldsymbol{P_1 = \nu\, e^{-E_1/kT}}$, where ν is a vibration frequency on the order of 10^{13} s^{-1}, k is the Boltzman constant, and T is the growth temperature. The reverse exchange from the surface to the buried layer is

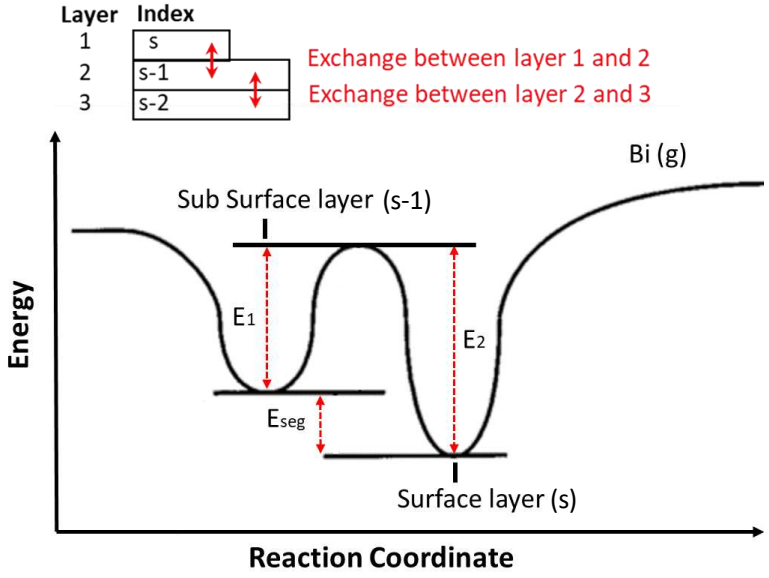

Figure 4: Reaction coordinate diagram showing the exchange energies of Bi between a surface layer and the lower layer.

also possible and is ruled by probability of exchange, P_2 defined as the same way. E_1 and E_2 are the barrier energies involved in the process (See Figure 4), related by $E_2=E_1+E_s$ where E_s is the segregation energy, defined by the energy difference between the atoms at the surface layer and the layer below [25]

$$E_s = (E_{Bi}^{s-1} - E_{Bi}^{s}) - (E_{As}^{s-1} - E_{Bi}^{s}) \quad (1)$$

Considering the growth of a single layer of InAsBi on a smooth InAs substrate, the model considers that, at the beginning of the deposition of every new monolayer (called s), the exchange initially occurs between the two upper layers of the substrate as shown in Figure 4. In these regions covered by the s-layer, exchanges between the s_{-1} and s_{-2} layers no longer occur because these layers are buried and the exchanges will probably no longer significantly reduce the free energy of the surface. Of course, in regions not yet fully covered, exchanges between layers s_{-1} and s_{-2} continue to occur. This action continues until the growth of the s-layer is complete. At that point, there is no longer any exchange between the s_{-1} and s_{-2} layer and the next layer begins to grow. The sequence of growth and exchange of the layers is repeated until the complete heterostructure is developed.

In this model, the physical processes to be taken into account are the deposition from the vapour phase, ϕ_{Bi}, the Bi content in every layer i, $\boldsymbol{x_{Bi}^{i}}$ and the exchanges between the three layers, $\boldsymbol{E_{i,i-1}}$. In this way, the main equations obtained through the development of this three-layer model are as follows:

$$\frac{dx_{Bi}^{s}}{dt} = \boldsymbol{\phi_{Bi}} + \boldsymbol{E_{s,s-1}},$$

$$\frac{dx_{Bi}^{s-1}}{dt} = \boldsymbol{E_{s-1,s}} + \boldsymbol{E_{s-1,s-2}},$$

$$\frac{dx_{Bi}^{s-2}}{dt} = \boldsymbol{E_{s-2,s-1}}, \quad (2)$$

Where

$$\boldsymbol{E_{i,i-1}} = \boldsymbol{P_1 x_{As}^{i} x_{Bi}^{i-1} - P_2 x_{As}^{i-1} x_{Bi}^{i}} \quad (3)$$

The coupled differential system (2) is resolved numerically layer by layer along the entire SL structure using a numerical Adams-Bashforth method. In the iterative calculus, once the layer s is completed, it becomes the new s_{-1} layer and so on. In addition, it is supposed that ϕ_{Bi} is constant during the InAsBi growth and becomes zero during the barrier growth. The fitting parameters are ϕ_{Bi}, P_1 and P_2. Figure 5 shows the experimental profiles of the

samples, together with the corresponding calculated profiles. The goodness of fit was evaluated using the coefficient of determination, R2. For Bi profiles above 200 data, the coefficient of determination is greater than 0.97 in all the cases.

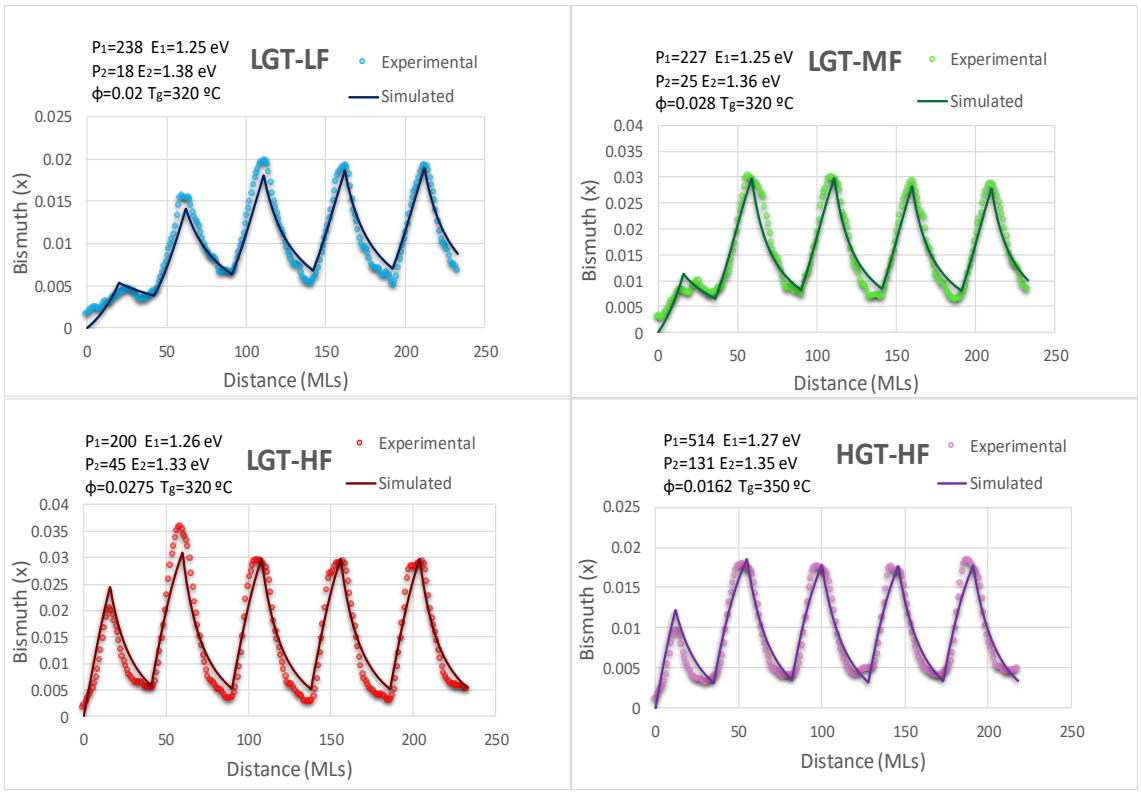

Figure 5: Experimental and calculated profiles of samples LGT-LF a), LGT-MF b), LGT-HF c) and HGT-HF d). The fitting parameters used in the model for each sample are included inside each plot.

The obtained ϕ_{Bi} parameter, defined as the incorporation rate of new Bi atoms at the surface, depends on the impinging flux but also on the sticking coefficient. In our case, the Bi impinging flux is controlled by the different beam equivalent pressures (BEPs) of Bi but the sticking coefficient could vary with factors such as growth rate, temperature or the presence of other elements. Thus, LGT-HF and HGT-HF, samples with the same BEP ($1.71 \times 10\text{-}7$ mBar) but grown at different substrate temperatures, give different ϕ_{Bi} parameters in the simulations, 0.0275 and 0.0162 s-1 respectively, indicating its strong influence on the sticking coefficient. During the growth of the first layer of InAsBi, the strong segregation of Bi results in a small incorporation into the bulk, but a large accumulation in the two upper layers (up to 16%). By cutting off the flux of Bi during the deposition of the InAs barrier, part of the Bi atoms on the surface slowly incorporate into the mass, but even so, there is still a high Bi content on the surface at the end of growth of this layer (about 4.9%). When the second layer of InAsBi begins to deposit, new Bi

atoms from the flux are added to the surface and this implies a greater exchange with the bulk. As consequence, at the end of the layer growth, the Bi content in the bulk reaches a higher value than in the first period (almost double). During the growth of the second InAs barrier, there is a higher incorporation of Bi, so that, at the end, the final content on the surface is around 5.2%. As the initial conditions are very similar to those of the second period, the third period follows the same trend and so on during the rest of the structure. Therefore, these results show that the segregation of bismuth in all samples could be described with a high precision with this model. Moreover, this approach makes it possible to determine the unknown exchange energies for this alloy, being E_1, 1.26 ± 0.01 eV and E_2, 1.36 ± 0.02 eV.

3.3. Segregation energies in III-V compounds.

Nowadays, experimental values for the exchange or activation energies have been obtained in different III-V systems such as In/Ga in InGaAs/GaAs [23], As/P in InGaP/GaAs [28], In/Al in InAs/AlAs [29], Sb/As in InAs/GaSb [30], Sb/As in GaAs/GaSb [31], Sb/As in GaAsSb/GaAs [27], Sb/As in InAsSb/InAs [32] and Bi/As in InAsBi/InAs (this work). In general, for a hypothetical ternary ABC compound alloyed from the binaries AB and AC, the energy barriers must be of the order of the binding energies of the binary compounds as the exchange process corresponds to the atomic motion of B and C atoms [23]. Some authors consider that the main contribution comes from the binding energy of the species that segregates, E_{AC} [29]. However, it seems logical that the differences of binding energy of the species of the matrix, E_{AB}, have a

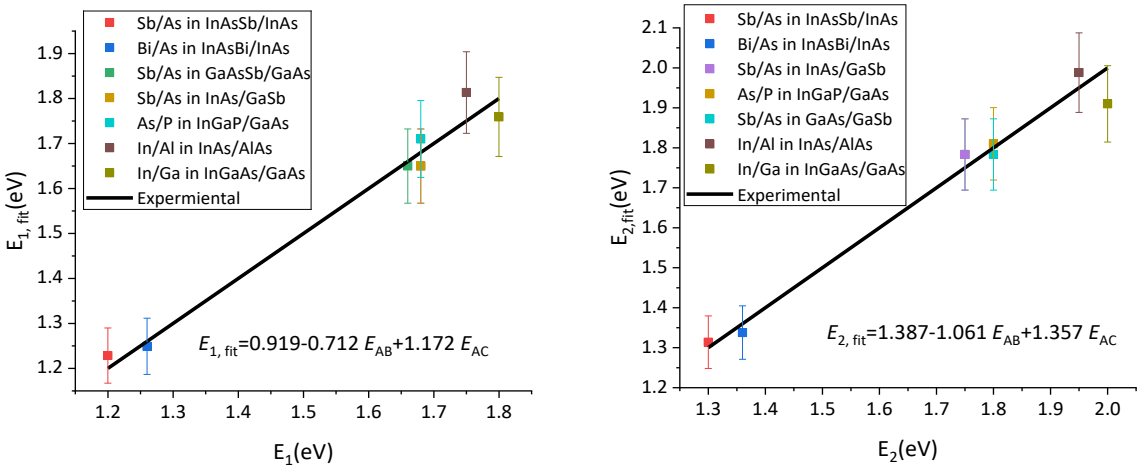

Figure 6. Plot of the fitted E_1 and E_2 energies versus the experimental ones for different segregation systems. The solid line represents equality between the calculated and measured energies.

significant contribution on these energies [31]. Our results show that a better fitting using experimental binding dissociation energies [33] is found when considering both energies.

In Figure 6, the calculated activation energies, E_1 and E_2, are plotted using the fitting parameters versus the experimental energies. The solid line of slope 1 represents the perfect matching between calculated and measured energies. The vertical distance of each point to the line can be associated with the error of the theoretical calculation compared to the measured result. As can be seen, though the contribution of E_{AC} in the calculus of the exchange energies is higher, the contribution of the E_{AB} component is also considerable. This relationship, therefore, allows predicting the value of the exchange energies for hitherto unknown III-V alloys such as Bi/As in GaAsBi/GaAs ($E_{1,fit}$=1.24 eV and $E_{2,fit}$=1.31 eV). However, we have not found any relationship between the binding energies and the segregation energies, E_s. As can be seen in eq. (1), in order to estimate the segregation energies, values of the energies of the atoms at the surface are needed. These data are very hard to obtain and compare among the different systems where a large variety of surface reconstructions are possible on (001) surfaces, depending on the growth conditions.

4. Conclusions.

InAsBi/InAs SLs samples have been grown free of dislocations and extended defects using different Bi fluxes and two growth temperatures. The growth temperature influences the way in which the bismuth is incorporated and its homogeneity, achieving better incorporation and greater homogeneity when the temperature is lower. At the lower growth temperature, the Bi profile reaches a plateau at about 3 %, showing more abrupt interfaces. Bi atoms suffer a strong segregation to the InAs barrier and Bi profiles along the growth direction have been successfully calculated using the three-layer exchange model. The exchange energies for As/Bi in InAsBi, E_1 and E_2, have been determined to be 1.26 eV and 1.36 eV, respectively. Finally, a relationship is found between the binding energies of the species implied in the exchange and the barrier energies for III-V alloys.

Acknowledgements

The work was supported by the Spanish Agencia Estatal de Investigación (AEI) and the European Regional Development Fund (ERDF) through project MAT2016-77491-C2-1-

R. The work of RDR was supported by the Royal Academy of Engineering under the Research Fellowships scheme.

References

[1] H. Huang, S. Tu, C. Zeng, T. Zhang, A.H. Reshak, Y. Zhang, Macroscopic Polarization Enhancement Promoting Photo- and Piezoelectric-Induced Charge Separation and Molecular Oxygen Activation, Angew. Chemie - Int. Ed. 56 (2017) 11860–11864. doi:10.1002/anie.201706549.

[2] F. Chen, H. Huang, L. Ye, T. Zhang, Y. Zhang, X. Han, T. Ma, Thickness-Dependent Facet Junction Control of Layered BiOIO3 Single Crystals for Highly Efficient CO2 Photoreduction, Adv. Funct. Mater. 28 (2018) 1–11. doi:10.1002/adfm.201804284.

[3] A. Duzik, J.C. Thomas, A. van der Ven, J.M. Millunchick, Surface reconstruction stability and configurational disorder on Bi-terminated GaAs(001), Phys. Rev. B. 87 (2013) 035313. doi:10.1103/PhysRevB.87.035313.

[4] B. Fluegel, S. Francoeur, a. Mascarenhas, S. Tixier, E. Young, T. Tiedje, Giant Spin-Orbit Bowing in GaAs1-xBix, Phys. Rev. Lett. 97 (2006) 067205. doi:10.1103/PhysRevLett.97.067205.

[5] K. Oe, Metalorganic vapor phase epitaxial growth of metastable GaAs1-xBix alloy, J. Cryst. Growth. 237 (2002) 1481–1485.

[6] S. Tixier, M. Adamcyk, T. Tiedje, S. Francoeur, a. Mascarenhas, P. Wei, F. Schiettekatte, Molecular beam epitaxy growth of GaAs[sub 1−x]Bi[sub x], Appl. Phys. Lett. 82 (2003) 2245. doi:10.1063/1.1565499.

[7] P.K. Patil, E. Luna, T. Matsuda, K. Yamada, K. Kamiya, F. Ishikawa, S. Shimomura, GaAsBi/GaAs multi-quantum well LED grown by molecular beam epitaxy using a two-substrate-temperature technique, Nanotechnology. 28 (2017). doi:10.1088/1361-6528/aa596c.

[8] Y. Tominaga, K. Oe, M. Yoshimoto, Low Temperature Dependence of Oscillation Wavelength in GaAs 1- x Bi x Laser by Photo-Pumping, Appl. Phys. Express. 3 (2010) 062201. doi:10.1143/APEX.3.062201.

[9] K.K. Nagaraja, Y.A. Mityagin, M.P. Telenkov, I.P. Kazakov, GaAs(1-x)Bix: A Promising Material for Optoelectronics Applications, Crit. Rev. Solid State Mater. Sci. 42 (2017) 239–265. doi:10.1080/10408436.2016.1186007.

[10] C. a Broderick, M. Usman, S.J. Sweeney, E.P. O'Reilly, Band engineering in dilute nitride and bismide semiconductor lasers, Semicond. Sci. Technol. 27 (2012) 094011. doi:10.1088/0268-1242/27/9/094011.

[11] H.Okamoto, K. Oe, Structural and Energy-Gap Characterization of Metalorganic-Vapor-Phase-Epitaxy-Grown InAsBi, Jpn. J. Appl. Phys. 38 (1999) 1022–1025. http://iopscience.iop.org/article/10.1143/JJAP.38.1022/pdf.

[12] P.T. Webster, A.J. Shalindar, N.A. Riordan, C. Gogineni, H. Liang, A.R. Sharma, S.R. Johnson, Optical properties of InAsBi and optimal designs of lattice-matched and strain-balanced III-V semiconductor superlattices, J. Appl. Phys. 119 (2016) 225701. doi:10.1063/1.4953027.

[13] Y. Tominaga, Y. Kinoshita, G. Feng, K. Oe, M. Yoshimoto, Growth of GaAs 1-x Bi x /GaAs multi-quantum wells by molecular beam epitaxy, Phys. Status Solidi. 5 (2008) 2719–2721. doi:10.1002/pssc.200779214.

[14] L. Dominguez, D.F. Reyes, F. Bastiman, D.L. Sales, R.D. Richards, D. Mendes, J.P.R. David, D. Gonzalez, Formation of Tetragonal InBi Clusters in InAsBi/InAs(100) Heterostructures Grown by Molecular Beam Epitaxy, Appl. Phys. Express. 6 (2013) 112601. doi:10.7567/APEX.6.112601.

[15] S.P. Svensson, H. Hier, W.L. Sarney, D. Donetsky, D. Wang, G. Belenky, Molecular beam epitaxy control and photoluminescence properties of InAsBi, J. Vac. Sci. Technol. B, Nanotechnol. Microelectron. Mater. Process. Meas. Phenom. 30 (2012) 02B109. doi:10.1116/1.3672023.

[16] A.G. Norman, R. France, A.J. Ptak, Atomic ordering and phase separation in MBE GaAs[sub 1−x]Bi[sub x], J. Vac. Sci. Technol. B Microelectron. Nanom. Struct. 29 (2011) 03C121. doi:10.1116/1.3562512.

[17] F. Bastiman, A.G. Cullis, J.P.R. David, S.J. Sweeney, Bi incorporation in GaAs(100)-2×1 and 4×3 reconstructions investigated by RHEED and STM, J. Cryst. Growth. 341 (2012) 19–23. doi:10.1016/j.jcrysgro.2011.12.058.

[18] D.F. Reyes, F. Bastiman, C.J. Hunter, D.L. Sales, A.M. Sanchez, J.P. David, D. González, Bismuth incorporation and the role of ordering in GaAsBi/GaAs structures, Nanoscale Res. Lett. 9 (2014) 23. doi:10.1186/1556-276X-9-23.

[19] R. Tsu, L. Esaki, Nonlinear optical response of conduction electrons in a superlattice, Appl. Phys. Lett. 19 (1971) 246–248. doi:10.1063/1.1653904.

[20] I.C. Sandall, F. Bastiman, B. White, R. Richards, D. Mendes, J.P.R. David, C.H. Tan, Demonstration of InAsBi photoresponse beyond 3.5 μm, Appl. Phys. Lett. 104 (2014) 171109. doi:10.1063/1.4873403.

[21] S.J. Pennycook, L.A. Boatner, Chemically sensitive structure-imaging with a scanning transmission electron microscope, Nature. 336 (1988) 565–567. doi:10.1038/336565a0.

[22] K. Muraki, S. Fukatsu, Y. Shiraki, R. Ito, Surface segregation of In atoms during molecular beam epitaxy and its influence on the energy levels in InGaAs/GaAs quantum wells, Appl. Phys. Lett. 61 (1992) 557–559. doi:10.1063/1.107835.

[23] O. Dehaese, X. Wallart, F. Mollot, Kinetic model of element III segregation during molecular beam epitaxy of III-III'-V semiconductor compounds, Appl. Phys. Lett. 66 (1995) 52–54. doi:10.1063/1.114180.

[24] J.M. Moison, C. Guille, F. Houzay, F. Barthe, M. Van Rompay, Surface segregation of third-column atoms in group III-V arsenide compounds: Ternary alloys and heterostructures, Phys. Rev. B. 40 (1989) 6149–6162. doi:10.1103/PhysRevB.40.6149.

[25] D.J. Godbey, M.G. Ancona, Modeling of Ge segregation in the limits of zero and infinite surface diffusion, J. Vac. Sci. Technol. A Vacuum, Surfaces, Film. 15 (1997) 976–980. doi:10.1116/1.580790.

[26] V. Haxha, I. Drouzas, J.M. Ulloa, M. Bozkurt, P.M. Koenraad, D.J. Mowbray, H.Y. Liu, M.J. Steer, M. Hopkinson, M.A. Migliorato, Role of segregation in InAs/GaAs quantum dot structures capped with a GaAsSb strain-reduction layer, Phys. Rev. B. 80 (2009) 165334. doi:10.1103/PhysRevB.80.165334.

[27] D.F. Reyes, V. Braza, A. Gonzalo, A.D. Utrilla, J.M. Ulloa, T. Ben, D. González, Modelling of the Sb and N distribution in type II GaAsSb/GaAsN superlattices for

solar cell applications, Appl. Surf. Sci. 442 (2018) 664–672. doi:10.1016/j.apsusc.2018.02.113.

[28] O. Dehaese, X. Wallart, O. Schuler, F. Mollot, X-ray photoemission characterization of interface abruptness and band offset of Ga0.5In0.5P grown on GaAs, J. Appl. Phys. 84 (1998) 2127–2132. doi:10.1063/1.368357.

[29] C. Dorin, J. Mirecki Millunchick, Lateral composition modulation in AlAs/InAs and GaAs/InAs short period superlattices structures: The role of surface segregation, J. Appl. Phys. 91 (2002) 237–244. doi:10.1063/1.1421240.

[30] R. Magri, A. Zunger, Effects of interfacial atomic segregation and intermixing on the electronic properties of InAs/GaSb superlattices, Phys. Rev. B. 65 (2002) 165302. doi:10.1103/PhysRevB.65.165302.

[31] T. Nakai, K. Yamaguchi, Analysis of Sb–As Surface Exchange Reaction in Molecular Beam Epitaxy of GaSb/GaAs Quantum Wells, Jpn. J. Appl. Phys. 44 (2005) 3803–3807. doi:10.1143/JJAP.44.3803.

[32] J.M. Millunchick, E.M. Anderson, C. Pearson, W.L. Sarney, S.P. Svensson, Incorporation kinetics in mixed anion compound semiconductor alloys, J. Appl. Phys. 114 (2013) 1–6. doi:10.1063/1.4849035.

[33] J.A. Kerr, D.R. Lide, CRC handbook of chemistry and physics 1999--2000: a ready-reference book of chemical and physical data, CRC Press Boca Raton, FL, USA, 2000.